JOURNAL OF CATALYSIS 5, 332–347 (1966)

Effectiveness of Large Catalyst Pellets—An Experimental Study

SEIYA OTANI AND J. M. SMITH

From the University of California, Davis, California

Received August 10, 1965; revised October 12, 1965

The effectiveness of the interior surface of porous catalyst pellets was studied by measuring rates of reaction for the oxidation of carbon monoxide. The data were obtained with 10% NiO-on-alumina catalyst for particles of catalyst and for 3/4-inch spherical pellets made from the particles.

Pellet rates of reaction per unit mass decreased with increasing pellet density as a consequence of the increased diffusion resistance. Rates per pellet showed a flat maximum as the density increased, as a result of the counter effects of increasing diffusion resistance and increasing surface area per pellet.

Attempts to predict the pellet rates of reaction from the particle rate data failed. Errors in diffusivities and the presence of a skin diffusion effect do not appear to explain the discrepancy between predicted and observed effectiveness factors. The blocking of micropores during the pelletting process is suggested as a contributing factor.

It is customary to evaluate the average rate of reaction in a porous catalyst pellet (prepared by compressing catalyst particles) by considering the diffusion and heat-transfer resistances within the pellet. From computations on this basis the composition and temperature are available at any point in the catalyst mass, and this information is used to establish the rate of reaction at that point. Integration of the rate–intraparticle position data gives the total rate for the pellet. This general approach has been used by many investigators (*1*, *2*, *6*, *7*, *14*, *15*, *16*, *20*, *22*) to develop methods of predicting the effectiveness factor (ratio of total rate to rate at pellet surface conditions) for the catalyst pellet. For a gaseous reaction involving a change in moles, intraparticle pressure gradients can also exist, but it has been shown (*9*) that this effect on E.F. is usually small.

Inherent in the described procedure is the premise that the rate of reaction on a catalyst particle is the same at any point in the pellet as long as the temperature and composition are the same. For this to be true the pelletting process must have no effect on the activity of the individual catalyst particle. Also, in order to obtain an explicit solution for E.F. it is customary to suppose that the effective diffusivity and thermal conductivity are the same throughout the pellet. The objective of the present study was to evaluate these assumptions, and the solution methods, by making a careful, experimental study of reaction rate on both particles and pellets. Large, spherical pellets (3/4-inch diameter) were used to emphasize the potential effects of nonuniform pelletting pressure. Also pellets of several densities were examined to determine the influence of the magnitude of the pelletting pressure. The final evaluation was made by comparing experimental and predicted effectiveness factors.

It has been established experimentally that concentration and temperature gradients can lead to effectiveness factors much less and also much greater than unity. For example, Cunningham *et al.* (*3*) measured rates of hydrogenation of ethylene on particles and pellets and found E.F. values from 0.2 to 10. However, it was not possible to compare these with predicted effectiveness factors, because the particle rate data was not known at all the compositions that

existed within the pellet. Also Rao (*11*) has measured pellet and particle rates for the orthohydrogen conversion using a Ni-on-Al_2O_3 catalyst. These isothermal data showed good agreement between predicted and experimental effectiveness factors. However the cylindrical pellets used were not subject to the stress existing in the preparation of spherical pellets. It is interesting to note that these authors' results for *large* Ni-on-silica-gel particles also agreed well with predicted E.F. values based upon rate data for small particles. Here, no pelletting process is involved and the assumptions of constant point rate of reaction and constant diffusivity and thermal conductivity are less uncertain.

For the experimental study the oxidation of carbon monoxide using a NiO on alumina catalyst was used. In addition to pellet rates and complete particle rate data, effective diffusivities and thermal conductivities are required to predict E.F. An average value of the diffusivity for the entire pellet was evaluated from data on diffusion in disk-shaped pellets of alumina (*19*). The thermal conductivity, again an average value for the whole pellet, was measured. Actually, it was found that the temperature gradients in the pellets were small enough to assume isothermal behavior. Hence the effective thermal conductivity was not needed to predict E.F., but proved useful in comparing maximum and actual temperature differences between the gas phase and center of the pellet.

Nomenclature

- A Outer surface area per unit volume of sphere $(cm)^{-1}$
- a Pore radius (cm)
- C Gas concentration (g moles/cm^3)
- D_e Effective diffusivity (cm^2/sec)
- E Activation energy (cal/g mole)
- F Total feed rate (g moles/sec)
- ΔH Enthalpy change of reaction (cal/g mole)
- h Thiele modulus, Eq. (11)
- k_e Effective thermal conductivity [cal/(sec)(cm)(°C)]
- M Molecular weight (g/mole)
- N Diffusion rate [moles/(sec)(cm^2)]
- R Radius of spherical pellet (cm)
- r Radial distance from center of pellet (cm)
- r_p Rate of reaction for unpelletted particles [g moles/(sec)(g cat.)]
- r_B Rate for pellet [g moles/(sec)(g cat.)]
- r°_p Rate of reaction for blocked particles in pellet [g moles/(sec)(g cat.)]
- T Temperature (°K)
- t Skin thickness around pellet (cm)
- V Pore volume [cm^3/(g cat.)]
- W Mass of catalyst (g)
- x Conversion of carbon monoxide
- y Mole fraction
- z Dimensionless distance, r/R
- β C/C_s
- γ Blocking factor defined by Eq. (15)
- ϵ Void fraction in pellet
- ρ Density [g/(cm^3)]

Subscripts

- a Macropore
- B Pellet
- C Center
- E Exit
- F Feed
- i Micropore
- p Particle
- s Surface of pellet, or solid
- sk Skin

Experimental

1. *Reaction Apparatus*

The assembly of apparatus for both particle and pellet rate measurements is shown schematically in Fig. 1. Highest purity gases (CO, 99.5%; O_2, 99.95%; CO_2, 99.99%) available in cylinders flowed through silica gel drier 4 to rotameters 5 and soap film meters 16. After mixing, 6, the reactants passed through preheater tube 8, filled with glass beads, and into reactor 9. Product gas from the reactor flowed through the sample side of thermal conductivity cell 15, while reactant gas passed through the reference side. The cell unbalance was thus a direct measure of the carbon dioxide formed. The cell, maintained at 25°C in constant temperature bath, 14, was operated at a constant current of 120 mamp. Calibration indicated that the cell emf was directly proportional to the mole

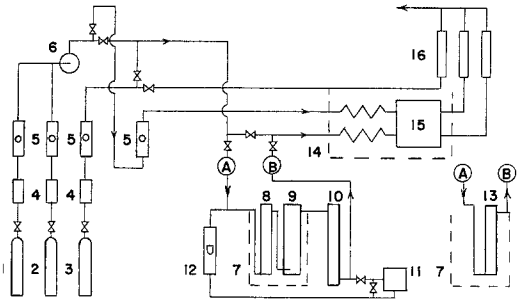

FIG. 1. Schematic diagram of apparatus. 1, 2 & 3. O_2, CO & CO_2 cylinders. 4. Driers (Silica gel). 5. Rotameters. 6. Gas mixer. 7. Heater. 8. Preheater. 9. Pellet reactor. 10. Cooler. 11. Recirculation pump. 12. Rotameter. 13. Particle reactor. 14. Constant temperature bath. 15. Thermal conductivity cell. 16. Soap film meters.

% CO_2 in the product gas, up to 8%. This relation was not affected by the CO–O_2 ratio up to 10 mole % CO in O_2.

The reactors were operated separately, and each was inserted in an electric heater, 7, whose temperature was adjusted by an input power controller equipped with a voltage stabilizer. A cylindrical copper sheet was between the heater and reactors to obtain a more uniform axial temperature profile.

The particle reactor, 13, is shown in detail in Fig. 2A. Catalyst particles, 100–170 mesh

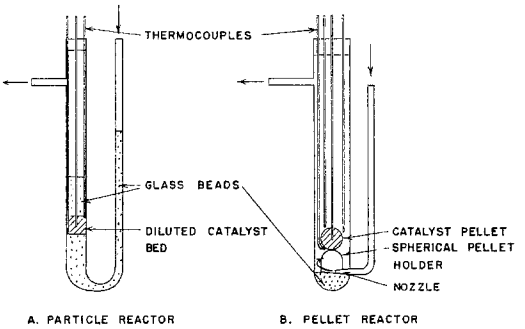

FIG. 2. Reactor details.

(88–149 micron) were diluted with glass beads (average diameter, 80 microns) and packed in a 1.6-cm. ID bed. The catalyst mass varied from 0.20 to 0.94 g and the glass beads were 2 to 10 times the volume of the catalyst, giving a bed height of about 1.5 cm. The diluted bed was supported by a bed of 470-micron glass beads as indicated in Fig. 2A. Temperatures were measured with three 30-gauge, copper-constantan thermocouples: one in the center of the catalyst bed, and the second and third in the outer diameter near the top and bottom of the bed. Preliminary tests showed that bare thermocouple junctions had some catalytic activity. Hence the couples were enclosed in fine glass capillaries (OD < 1 mm). No conversion was detected in the apparatus containing glass beads and thermocouple capillaries, but no catalyst.

For the pellet measurements the reactants passed from the preheater into a tank-flow reactor, 9, made from 2.9-cm ID glass tubing. To eliminate dead space and increase turbulence, the end of the tube was sealed and filled with glass beads as indicated in Fig. 2B. The catalyst pellet rested on a glass hemisphere and was held in vertical alignment by the thermocouple capillary extending to the center of the pellet. The gases from the preheater, 8, entered the reactor tangentially through a nozzle. The reactor was operated as a recycle type by using a neoprene diaphragm pump, 11. The normal feed rate of reactants was 0.5 cm^3/sec (25°C, 1 atm). The recirculation rate could be varied from 0 to 25 cm^3/sec, thus giving a maximum recycle ratio of 50.

Three glass-enclosed, copper-constantan thermocouples (30 ga.) were inserted in the gas around the pellet at locations shown in Fig. 2B. The junctions were approximately 1 mm from the pellet surface. A 1-mm diameter hole was drilled in the pellet and a fourth thermocouple, enclosed in glass, was inserted to the center. The entire reactor was covered with aluminum foil to reduce temperature gradients. Preliminary tests using no catalyst pellet, but including thermocouples, showed no activity.

The magnitude of temperature gradients and conclusions regarding mixing, are discussed in the next section.

2. *Catalyst Preparation*

A single batch of 10 wt % NiO on Al_2O_3 was prepared by soaking boehmite ($Al_2O_3 \cdot H_2O$) powder in $Ni(NO_3)_2$ solution. After

impregnation, the material was dried at 110°C for 2 hr and then maintained at 450°C for 4 hr. The decomposition temperatures of boehmite and $Ni(NO_3)_2$ to NiO are reported (*5*) as 360°C and 400°C. The reduced catalyst was subjected to a mild grinding operation to reproduce approximately the size distribution of the original boehmite powder.

For the particle reactor the catalyst was sieved and the 100–170 mesh size range used. For pellets the particles were compressed into a spherical steel mold. The metal surface of the mold was lubricated with a very thin layer of stearic acid. The stearic acid adhering to the pellet surface was later evaporated during catalyst pretreatment at 370°C. The small space surrounding the thermocouple capillary inserted in the pellet was filled with catalyst particles. No cementing material was used to prepare the pellets.

3. *Physical Properties of Catalyst*

The effective diffusivity depends upon porosities and pore-size distribution in the pellet. This information was measured for the micropores within the catalyst particles and for the macropores between the particles. The micropore (<150 Å) data were obtained by N_2 adsorption using a Perkin-Elmer Sorptometer. The method and its limitations have been described elsewhere (*11*). The macropore (>150-Å radius) properties were measured by mercury penetration using a porosimeter (*11*). The samples used contained material extending from the surface to the center of the pellet. This was done to obtain average properties in the event that there was a significant variation, in porosity for example, across the radius of the pellet. The samples for the porosimeter were first dried at 110°C for 2 hr, while those for the Sorptometer were degassed at 370°C *in situ* for 2 hr in a stream of helium. Ten samples of four density levels were used in the porosimeter, while one sample at each density was studied in the Sorptometer.

Typical pore-volume distribution curves are shown in Fig. 3 and porosity and mean pore radii data are summarized in Table 1. The macro and micro mean pore radii were evaluated from the following equations,

TABLE 1
GEOMETRICAL PROPERTIES OF CATALYST PELLETS

Pellet No.	Pellet density[a] ρ_B (g/cm³)	Pore volume[a] (cm³/g) Macro V_a	Micro V_i	Void fraction[b] ϵ_a	ϵ_i	ϵ_s	Mean pore radius (A°) $\bar{a}_a$	$\bar{a}_i$	Solid density[c] ρ_s [g/(cm³)]
1-a	0.680	0.734	0.350	0.499	0.238	0.263	6450	35	2.58
b	0.675	0.775	0.350	0.524	0.236	0.240	7770	35	2.81
c	0.672	0.678	0.350	0.466	0.235	0.299	7600	35	2.25
Average	0.68	—	0.350	0.496	0.236	0.268	7270	35	2.55
2-a	0.790	0.582	0.344	0.460	0.272	0.268	3530	34	2.95
b	0.790	0.599	0.344	0.473	0.272	0.255	4050	34	3.10
Average	0.79	—	0.344	0.466	0.272	0.262	3790	34	3.03
3-a	0.893	0.469	0.336	0.419	0.300	0.281	2040	32	3.18
b	0.923	0.436	0.336	0.402	0.310	0.288	1900	32	3.20
Average	0.91	—	0.336	0.410	0.305	0.285	1970	32	3.19
4-a	1.11	0.317	0.333	0.352	0.370	0.278	1500	31	3.99
b	1.11	0.305	0.333	0.338	0.370	0.292	1270	31	3.80
c	1.11	0.306	0.333	0.340	0.370	0.290	1050	31	3.83
Average	1.11	—	0.333	0.343	0.370	0.287	1270	31	3.87

[a] The densities and pore volumes are based upon one gram of used catalyst.
[b] $\epsilon_a = V_a\rho_B$; $\epsilon_i = V_i\rho_B$; $\epsilon_s = 1 - (\epsilon_a + \epsilon_i)$.
[c] $\rho_s = \rho_B/\epsilon_s$

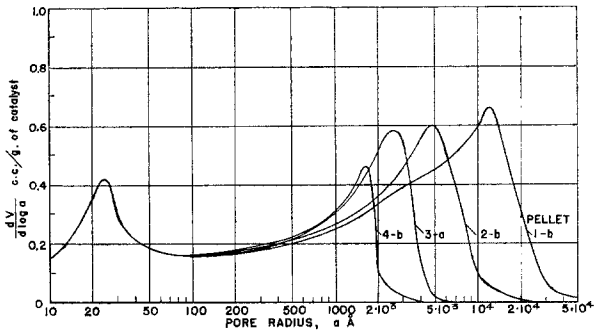

FIG. 3. Pore-size distribution of catalyst pellets.

based upon an average with respect to volume:

$$\bar{a}_a = \int_0^{V_a} a_a dV_a \Big/ V_a \qquad (1)$$

$$\bar{a}_i = \int_0^{V_i} a_i dV_i \Big/ V_i \qquad (2)$$

The micropore curves were essentially the same for all densities up to 90 Å. Therefore the surface areas of all pellets were about the same, 256 cm^2/g. As Fig. 3 shows, the macropore volume decreased with increasing density. The data in Table 1 indicate that small changes in density around a given level can result in rather large changes in macrovoid fraction and $\bar{a}_a$. The solid density calculated from pellet density and solid void fraction increases with pellet density. This suggests that there is some change in pore structure with density that is not reflected in the measurements. For example, the Sorptometer and porosimeter methods do not account for dead-end pores. Variations in the extent of these pores with pellet density would affect the calculated solid density.

4. *Thermal Conductivity*

The thermal diffusivity of the pellets was measured approximately using the unsteady heating technique described by Cunningham *et al.* (*3*). The effective thermal conductivity was then calculated from the known pellet density and a specific heat predicted from the composition and specific heats of the elements involved. Five pellets of different density were made specifically for these measurements. The results are given in Table 2.

TABLE 2
EFFECTIVE THERMAL CONDUCTIVITY OF CATALYST PELLETS AT 300°C

Pellet density (g/cm^3)	$k_e \times 10^4$ [cal/(sec) (cm) (°C)]
0.66	2.9
0.67	2.7
0.775	2.9
0.95	3.6
1.14	4.0

These k_e values were determined with air-filled pores. Under reaction conditions the pores would contain primarily oxygen with small amounts of CO and CO_2. Judging from the work of Mischke (*8*) this difference in gas composition would be less than the errors involved in the experimental method. The level of k_e in Table 2 is comparable to that for $Al_2O_3 \cdot H_2O$, as determined by Mischke and demonstrates again the low conductivities of pellets prepared from microporous particles.

CATALYST PRETREATMENT AND ACCURACY OF RATE MEASUREMENTS

When a fresh sample of catalyst particles was charged, accumulated water vapor was removed by passing a stream of O_2 through the reactor for 2 hr at 370°C. If reaction was then initiated by adding a CO-O_2 stream, the rate gradually decreased with time. After 25 hr the activity was reduced about 30%. This behavior, also observed by Parravano and Boudart (*10*) and by Winter (*23*), apparently is due to retardation by CO_2. It was found that after drying at 370°C and a

CO_2 pretreatment, a reproducible and constant rate could be achieved (for 60 hr). The pretreatment consisted of passing a stream of reactants containing 3 mole % CO_2 over the catalyst for 1 hr at 250°C. It was also observed that the activity of a fresh catalyst *pellet* decreased with on-stream time, but that a pretreatment of 2 hr at 250°C with a gas stream containing 3 mole % CO_2 was sufficient to ensure a constant rate thereafter. These procedures were used before obtaining the rate data reported later.

The thermocouples were calibrated with a standard thermometer and only those which read within 0.1°C of each other were used. The three temperatures in the particle reactor differed by less than 4°C for all the runs, with the values increasing in the direction of flow. Hence the temperature corresponding to the measured rate was taken as the arithmetic average of the three readings.

In the pellet reactor, preliminary runs with a feed of pure oxygen showed differences as high as 2°C between the four thermocouples. The three gas temperatures were higher than the pellet-center value, and the lowest gas thermocouple (see Fig. 2B) gave the highest reading. This small variation appeared to be due to different radiation effects at different positions in the reactor. A correction factor chart was prepared over the range 250–375°C to account for this variation. To test the validity of the pellet-center readings, measurements were made with both a bare and a glass-insulated thermocouple inserted in the pellet with pure oxygen flow at reaction temperature. The two readings were within 0.2°C of each other. It was concluded that the catalytic activity of the bare thermocouple, while influencing the rate data, did not affect the temperature measurement significantly. The final data were obtained with glass-enclosed thermocouples.

To test the possible effect of the stearic acid in the pellet mold, particle rate data were also measured by using used catalyst particles. These were prepared by breaking and sieving a used pellet. The rates so obtained were within 10% of the fresh catalyst data over the complete temperature range.

The final particle rate data consisted of 143 runs taken with eight different samples of catalyst over the time period of the investigation. At the same conditions, the maximum deviation of measured rates was about 10%. The reproducibility is illustrated in Fig. 4 at 350°C and 370°C. The deviations

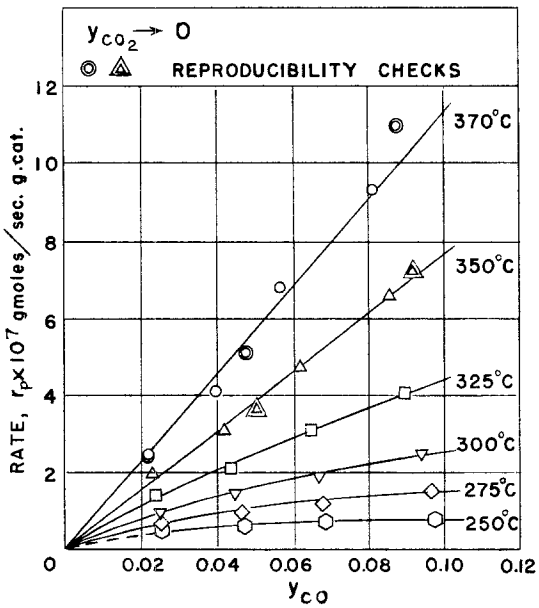

FIG. 4. Particle rate data at $y_{CO_2} \rightarrow 0$.

were largest at the lowest temperatures and CO composition where the low level of the rate reduced the accuracy of measurement.

The final pellet data consisted of 107 runs on 10 pellets of four density levels. The pellet data scattered more than that for particles and reached 30% deviation for the highest density pellets. The deviations showed no trend with time or pellet, and appeared to be random fluctuations caused by variations in pellet structure.

Rate Data

The reactors were operated at atmospheric pressure and from 250° to 375°C. The gas in the pellet reactor was maintained at about 6 mole % CO with varying amounts of CO_2 depending upon the rate of reaction. In order to duplicate all conditions in the pellet, rates for the particles were measured over a composition range: 1–11 mole % CO, 0–8 mole % CO_2, remainder O_2.

1. *Particle Results*

The particle-to-tube-diameter ratio in the reactor (Fig. 2A) was small enough to assure uniform velocity across the catalyst bed. Further the length-to-diameter ratio of the bed was small (about 1.0). Hence plug-flow behavior was assumed. The conversion of CO was usually held to a low value so that the rate could be taken as constant in the bed and associated with an arithmetic average of inlet and exit compositions (differential reactor operation). At the highest temperatures the conversion in some of the runs reached 40%. However, at these conditions the rate is first order so that the correct average composition to associate with the rate is the logarithmic mean of the entering and exit values. As noted earlier the temperature variations were always small enough to assign an arithmetic average value to the bed.

The expression for the rate in a differential reactor in terms of feed and exit CO_2 mole fractions is

$$r_p = \frac{F}{W} \frac{(y_{CO_2})_E - (y_{CO_2})_F}{[1 + \frac{1}{2}(y_{CO_2})_E][1 + \frac{1}{2}(y_{CO_2})_F]} \quad (3)$$

Sample rates calculated from this equation are shown in Table 3 and more complete data illustrated in Figs. 4–7 for two levels of CO_2 concentration. Similar data were obtained up to 8% CO_2.

The flow rate was varied from 0.3 to 0.50 cm^3/sec (25°C, 1 atm) and over this range the rate was constant. Also the estimated concentration change between bulk gas and particle surface, using available mass-transfer coefficients, was negligible. These results suggested that external diffusion resistances were not involved at the operating conditions.

Figures 4 ($CO_2 \rightarrow 0\%$) and 5 ($CO_2 = 6\%$) show that the rate was first order with respect to CO at 370°C, and independent of CO_2 concentration. At lower temperatures Fig. 4 indicates a CO order less than unity.

TABLE 3
Illustrative Rate Data for Particles

Mass of catalyst (g)	Run no.	Feed rate[a] (cm^3/sec)	Gas composition (mole %) CO Feed	CO Exit	CO_2 Exit	Conversion x	$r_p \times 10^7$ [g moles/(sec)(g)]	$\bar{t}$ (°C)
0.625	1	0.30	5.0	4.1	0.92	0.183	1.8	311
	2	0.30	5.0	3.6	1.5	0.298	3.0	333
	3	0.30	5.0	3.1	2.0	0.396	4.3	360
	4	0.30	5.0	4.4	0.60	0.120	1.2	283
0.938	6	0.45	5.0	4.0	1.1	0.219	2.0	316
	7	0.45	5.0	4.4	0.67	0.134	1.3	288
	8	0.45	5.0	4.7	0.34	0.068	0.66	253

[a] At 25°C, 1 atm.

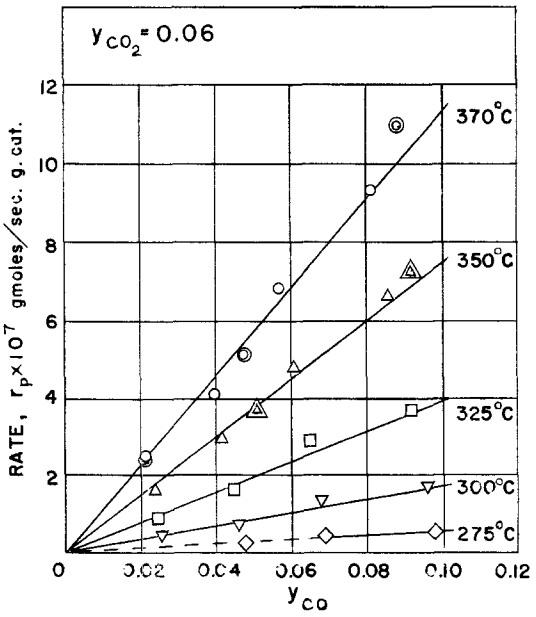

FIG. 5. Particle rate data at $y_{CO_2} = 0.06$.

Also comparison of points on Figs. 4 and 5 shows that CO_2 retards the rate at lower temperatures. This behavior is in general agreement with previous literature on the kinetics of this reaction on a NiO catalyst. Parravano and Boudart (*10*) found that the CO order was 1.0 above 200°C but dropped to 0.5 in the range 106–174°C. Wagner *et al.* (*17*) reported that the reaction was first order at 715°C.

The Arrhenius plot in Fig. 6 ($CO_2 \rightarrow 0\%$) gives activation energies increasing from 11.1 to 13.7 kcal/g mole with CO mole fraction. Parravano (*10*) found 13.7 kcal/g mole at 180–250°C. However Keier *et al.* (*4*) reported 4.5 kcal/g mole. The strong retardation effect of CO_2 at low temperatures is clearly evident in Fig. 7 where the Arrhenius lines show an apparent activation

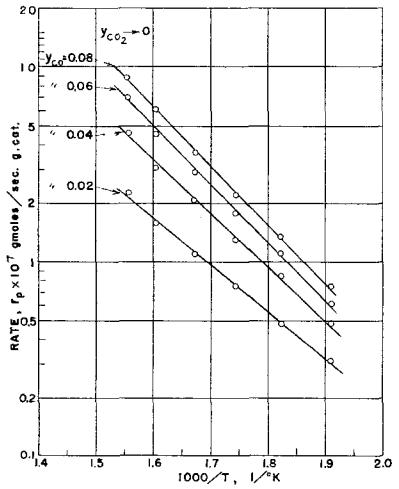

FIG. 6. Particle rate data; Arrhenius plot for $y_{CO_2} \rightarrow 0$.

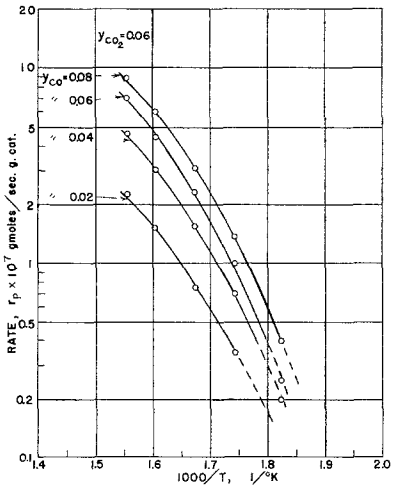

FIG. 7. Particle rate data; Arrhenius plot for $y_{CO_2} = 0.06$.

energy which increases as the temperature falls.

2. *Pellet Results*

In introductory tests the pellet reactor was operated at recycle rates from 0 to 25 cm³/sec with a constant feed rate of 0.5 cm³/sec. Above 15 cm³/sec the rate was constant. To evaluate further the influence of external diffusion resistance, the change in CO concentration between bulk gas and pellet surface was estimated using mass-transfer coefficients reported by Wakao *et al.* (*18*). At the most severe condition, 370°C, this change was 1.3% of the surrounding gas concentration. Furthermore, the apparent activation energy for the pellet data did not decrease at the highest temperatures (Fig. 8). A decrease would be expected if external diffusion resistance was contributing to the rate. The absence of these effects is due to the relatively low level of the rate for this reaction.

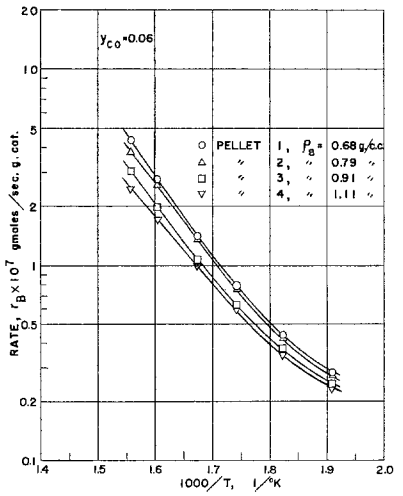

FIG. 8. Pellet rate data for $y_{CO} = 0.06$.

The temperature of the center of the pellet was always greater than the three gas temperatures (Fig. 2B). The gas temperatures were generally about the same; the maximum difference between them was 3°C. The center temperature was up to 7°C above the average of the gas temperatures and this maximum difference occurred at the 370°C level. Temperature differences of this magnitude, combined with the comparatively low activation energy for the reaction, are insufficient to introduce a significant nonisothermal effect on the effectiveness factor for the pellet. This can be quantitatively checked in an approximate way using the charts of Weisz and Hicks (*20*). In view of these conditions, the pellet system was treated as an isothermal stirred-tank reactor with complete mixing. Since the feed to the reactor contained no CO_2, the pellet rate, per gram of catalyst, could be calculated from

$$r_B = \frac{F}{W} \frac{(y_{CO_2})_E}{1 + \frac{1}{2}(y_{CO_2})_E} \qquad (4)$$

The rate so calculated was assigned a temperature equal to the average of the pellet-center and average-gas temperatures.

The gas composition and temperature around the pellet were dependent upon the rate of reaction as well as on the feed-gas composition. Hence it was not possible to operate at a preassigned composition. Rather 6% CO and 370°, 350°, 325°, 300°, 275°, or 250°C were chosen as the fixed points upon which to base the effects of pellet density. Runs were made over a range of feed composition and temperature levels and the data interpolated to the fixed points. Figure 8 shows the results for the pellets of four different densities.

The rate per gram decreases as the density increases, indicating that the interior of the pellet is less available at higher densities. This is expected since the macro porosity and pore size decrease, causing the diffusion resistance to increase, as the density goes up. The same trend was found by Cunningham (*3*). From a design viewpoint the rate per pellet is also of interest since this establishes the reactor volume in a fixed-bed reactor. Considered on this basis the rate goes through a rather flat maximum at high temperatures, but is approximately constant at low temperatures. The possibility of an optimum catalyst density has been observed previously (*3*) and can be explained by the counter effects of increasing diffusion resistance and increasing mass (and hence surface) of catalyst as the density increases.

The shape of the curves in Fig. 8 is dif-

ferent than expected for a first order, diffusion-restricted system. For such a case the apparent activation energy decreases as the temperature increases. The opposite effect is observed in Fig. 8 because CO_2 retards the point rate and this decrease is a strong function of the CO_2 concentration. The mole fraction CO is fixed at 6%. The mole fraction CO_2 increases as the temperature increases, because the rate goes up. Hence the point rate is retarded more at intermediate temperatures than at the lowest ones. This more than offsets the increased importance of diffusion, so that there is a smaller increase in *pellet* rate than expected. Of course at the highest temperature, 370°C, the point rate is independent of CO_2, and the retardation effect no longer exists. The pellet rate lines are approximately straight at this temperature in Fig. 8, but presumably they would show the expected decrease in activation energy for a first order reaction at higher temperatures.

Experimental Effectiveness Factors

Provided the rate in a catalyst particle in the pellet is the same as in a loose assembly of particles, the effectiveness factor is simply the ratio of the pellet and particle rates. The comparison should be made at the composition and temperature of the gas surrounding the pellet. This corresponds to 6.0 mole % CO and different amounts of CO_2 depending upon the pellet density and temperature level. The particle rate data are available at all these conditions so that E.F. values can be evaluated. The results are given in Table 4. The effectiveness factors are low, documenting the importance of diffusion resistance under these conditions. E.F. decreases with density, as expected from the earlier discussion. Also the values increase slowly with temperature. This is the opposite of normal expectations; the rate might be expected to increase with temperature, thus leading to a more significant diffusion resistance and lower E.F. However, as temperature increases the CO_2 concentration also increases, as noted from the data shown in the table. The CO_2 retards the point rate and therefore the diffusion resistance decreases as the temperature rises. The retardation becomes unimportant at 370°C and it is noted that E.F. does not

TABLE 4

Pellet Rate Data and Experimental Effectiveness Factors[a]

Pellet No.		Temperature (°C)				
		370°	350°	325°	300°	275°
1	$r_B \times 10^7$	4.3	2.7	1.4	0.78	0.44
$\bar{\rho}_B = 0.68$	$(y_{CO_2})_B$%	5.1	3.2	1.7	0.91	0.51
	$r_p \times 10^7$	6.7	4.5	2.6	1.6	1.0
	$(E.F.)_{exptl}$	0.64	0.60	0.54	0.49	0.44
2	$r_B \times 10^7$	3.8	2.5	1.4	0.77	0.43
$\bar{\rho}_B = 0.79$	$(y_{CO_2})_B$	5.3	3.6	1.9	1.1	0.58
	$r_p \times 10^7$	6.7	4.5	2.6	1.6	0.97
	$(E.F.)_{exptl}$	0.57	0.56	0.54	0.48	0.44
3	$r_B \times 10^7$	3.0	2.0	1.1	0.63	0.37
$\bar{\rho}_B = 0.91$	$(y_{CO_2})_B$	4.8	3.2	1.8	1.0	0.59
	$r_p \times 10^7$	6.7	4.5	2.6	1.6	0.96
	$(E.F.)_{exptl}$	0.45	0.44	0.42	0.39	0.39
4	$r_B \times 10^7$	2.5	1.7	1.0	0.59	0.35
$\bar{\rho}_B = 1.11$	$(y_{CO_2})_B$	4.9	3.3	2.0	1.1	0.67
	$r_p \times 10^7$	6.7	4.5	2.6	1.6	0.94
	$(E.F.)_{exptl}$	0.37	0.38	0.38	0.37	0.37

[a] Rates are g moles/(sec)(g). All data for $y_{CO} = 0.06$. $(E.F.)_{exptl} = r_B/r_p$

increase significantly between 350° and 370°C.

Computed Effectiveness Factors

For the nearly isothermal conditions prevailing in this study, the prediction of the effectiveness factor requires only a differential mass balance of CO within the pellet. Due to the small mole fraction CO, the change in moles as a result of reaction, and accompanying change in total pressure within the pellet, will have a negligible effect (*9*). The experimental conditions indicated no external diffusion resistance so that the gas composition at the surface of the pellet could be equated to the bulk gas composition.

Even with these simplifications two key assumptions are necessary to predict E.F. The first is that the effective diffusivity is uniform throughout the pellet. The second is that the activity of the catalyst is the same throughout the pellet and equal to that of the unpelletted catalyst particles. Then the dimensionless form of the mass balance may be written

$$\frac{d^2\beta}{dz^2} + \frac{2}{z}\frac{d\beta}{dz} = r_p\rho_B \frac{R^2}{D_e C_s} \tag{5}$$

with boundary conditions

$$z = 1, \qquad \beta = 1 \tag{6}$$

$$z = 0, \qquad d\beta/dz = 0 \tag{7}$$

and where

$$\beta = C/C_s$$

$$z = r/R$$

The effectiveness factor is given by

$$(\text{E.F.})_{\text{calc.}} = \int_0^R 4\pi r^2(\rho_B r_p)dr \Big/ \frac{4}{3}\pi R^3 \rho_B (r_p)_s = \frac{3}{(r_p)_s}\int_0^1 z^2 r_p dz \tag{8}$$

Equations (5–7) are solvable numerically for any form of the rate expression. The resulting concentration profiles are sufficient to establish r_p at any radial position for use in Eq. (8). In this way $(\text{E.F.})_{\text{calc}}$ can be calculated if D_e and $r_p = f$ (composition) are known. If the rate is first order, analytical solution is possible. Thiele (*14*) gives the results

$$\beta = \frac{\sinh(hz)}{z\sinh(h)} \tag{9}$$

$$(\text{E.F.}) = \frac{3}{h^2}\left[\frac{h}{\tanh h} - 1\right] \tag{10}$$

$$h = R\left[\frac{(r_p)_s\rho_B}{C_s D_e}\right]^{1/2} \tag{11}$$

In the numerical solution of Eq. (5) a trial and error procedure is required, because the boundary conditions do not apply for the same location in the pellet. The method used was to assume $d\beta/dz$ at $z = 1$, carry out the stepwise calculations, and then note if the boundary condition at the center of the pellet, Eq. (7), was satisfied. At 370°C, the reaction was first order in CO with no effect of CO_2 so that Eq. (9) was applicable. This provided a means of checking the numerical method of solution. In most cases, five radial increments and the inclusion of the second derivitive term in the Taylor expansion were sufficient to give reliable concentration profiles.

The mole fraction of CO_2 within the pellet was necessary in order to evaluate r_p at all temperatures except 370°C. This was computed by assuming stoichiometric diffusion, i.e., $(N)_{CO_2} = -(N)_{CO}$. Then if the diffusivities are independent of radial position, the mole fraction CO_2 in terms of the known y_{CO} is

$$y_{CO_2} = (y_{CO_2})_s + \frac{(D_e)_{CO}}{(D_e)_{CO_2}}\left[(y_{CO})_s - y_{CO}\right] \tag{12}$$

where

$$\frac{(D_e)_{CO}}{(D_e)_{CO_2}} = \left[\frac{M_{CO_2}}{M_{CO}}\right]^{1/2} \tag{13}$$

This last expression has been justified experimentally and theoretically for both Knudsen and bulk diffusion in porous media.

For the E.F. calculated first it was supposed that the two key assumptions are valid. Also it was supposed that the diffusivity for the spherical pellets was the same as that available from diffusion data (*19*) in disk-shaped pellets of alumina. These latter experimental data were correlated in Ref. (*19*) using a so-called random-pore model which includes the effects of bulk and

Knudsen diffusion in macropores and micropores. Table 5 summarizes the diffusivities

TABLE 5
EFFECTIVE DIFFUSIVITY FROM DIFFUSION DATA[a]

Pellet No.	Temperature (°C)				
	370°	350°	325°	300°	275°
1	0.16	0.15	0.14	0.13	0.13
2	0.12	0.12	0.11	0.10	0.10
3	0.076	0.073	0.070	0.066	0.063
4	0.045	0.044	0.042	0.041	0.039

[a] Diffusivities in cm²/sec. Diffusion data from ref. 19.

so obtained. Illustrative concentration and rate profiles determined using these D_e values are shown in Fig. 9.

the predominance of the effect of temperature on the particle rate of reaction.

The difference between experimental and calculated E.F. suggests uncertainties in the prediction method, for the differences are beyond the expectations from experimental errors. Therefore, the explanation should be sought in terms of the deviations from the key assumptions in the prediction method.

1. *Potential Diffusivity Errors*

The use of a constant D_e throughout the radius of a spherical pellet, prepared by applying a force to the outer surface, is open to question. Satterfield and Saraf (*13*) have reported several-fold changes in experimental diffusivities with axial distance in disk-shaped pellets, presumably due to variations

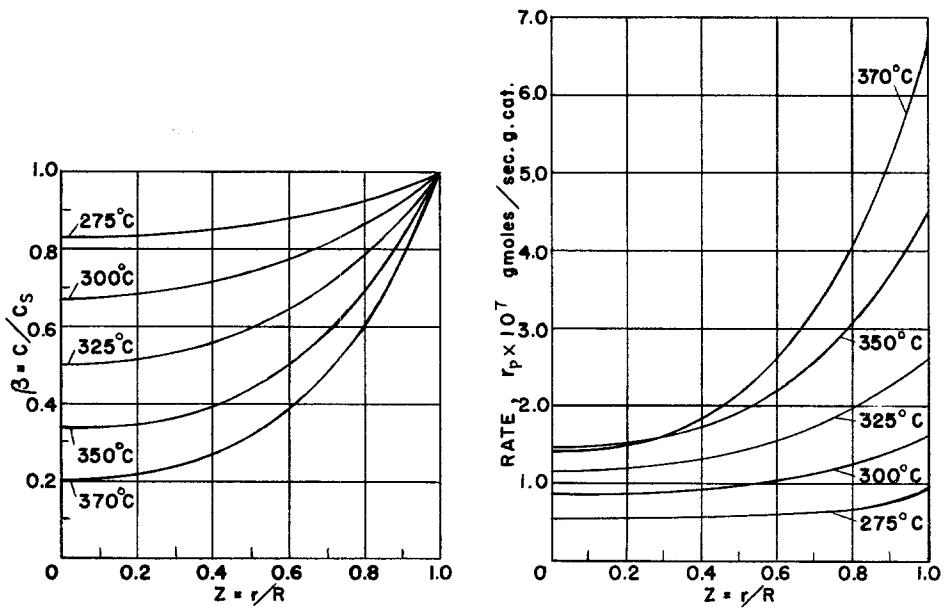

FIG. 9. Intrapellet concentration and rate profiles for Pellet 4.

The calculated E.F. (lines #1) are compared with the experimental values for the pellets of extreme densities in Figs. 10 and 11. For both densities the calculated results are higher than the experimental values, although the trend with temperature is similar. The unusual decrease in E.F. as the temperature goes down has been explained earlier. The initial increase in $(\text{E.F.})_{\text{calc}}$ as the temperature drops from 370°C is due to in stress and particle characteristics. Even larger changes might be expected for spherical pellets, because of the potentially larger variations in stress.

It is instructive to calculate the D_e values that would give agreement between calculated and experimental E.F., still assuming a constant diffusivity. This can be done easily at 370°C from Eqs. (10) and (11) since at this temperature first-order kinetics

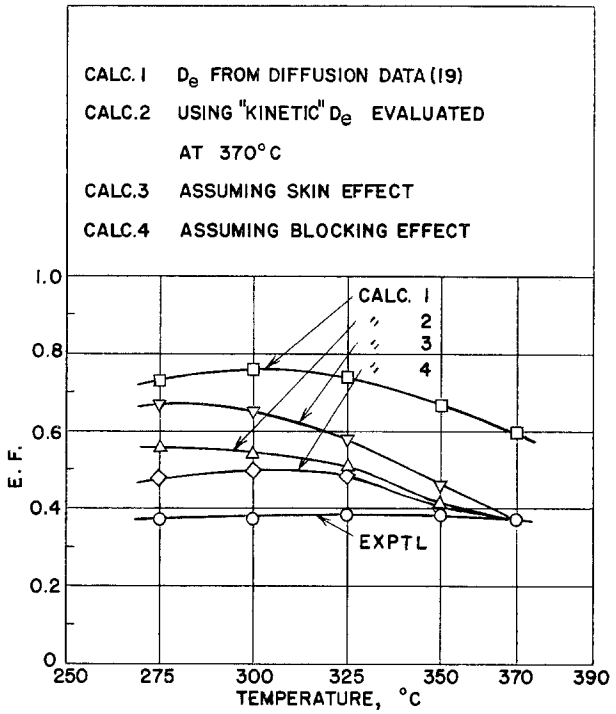

FIG. 10. Experimental and calculated E.F. for Pellet 4.

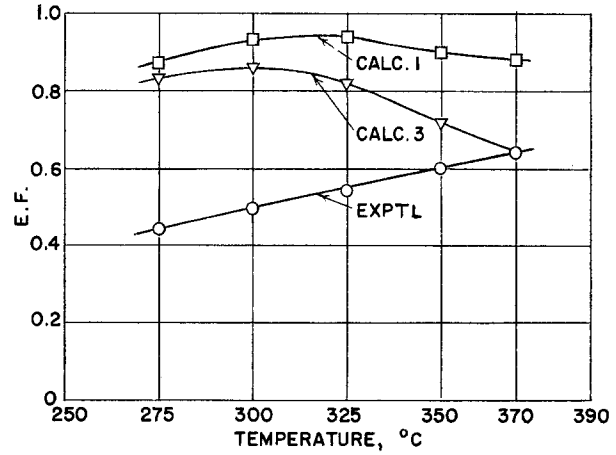

FIG. 11. Experimental and calculated E.F. for Pellet 1.

was observed. The resulting "kinetic" diffusivities are compared with the values from diffusion data in Table 6. These results indicate that if all the errors were due to the diffusivity, the D_e based upon diffusion in disks is four to fivefold too high. Using the value of 0.27 for Pellet 4, E.F.'s were calculated for the entire temperature range. The

TABLE 6
DIFFUSIVITY RATIOS AT 370°C

Pellet No.	$(D_e)_{kinetic}/(D_e)_{diff}$
1	0.21
2	0.23
3	0.22
4	0.27

results are designated by curve 2 in Fig. 10. The enforced agreement with $(E.F.)_{exptl}$ at 370°C is seen not to hold at lower temperatures. Both this lack of agreement and the small ratios in Table 6 suggest that diffusivity errors cannot explain the entire deviation between curve 1 and $(E.F.)_{exptl}$.

It is conceivable that the pellet mould could produce a thin outer layer of catalyst that had a much lower diffusivity than the inner material. Assuming that such a low-diffusivity skin is responsible for all the errors, a skin thickness-to-diffusivity ratio can be evaluated at 370°C, where first order kinetics apply. Cunningham *et al.* (*3*) developed the following equation for this situation:

$$(E.F.)_{exptl} = \frac{(E.F.)_{core}}{1 + [t/A(D_e)]_{sk}(E.F.)_{core}[\rho_B(r_p)_s/C_s]} \quad (14)$$

Here $(E.F.)_{core}$ is the effectiveness factor for all of the pellet except the outer skin. It is the same as $(E.F.)_{calc}$ for curve 1 in Fig. 10. The overall E.F. is taken equal to the experimental value. It differs from $(E.F.)_{core}$ depending upon the $t/(D_e)_{sk}$ ratio. For pellet 4 at 370°C, $[t/A(D_e)]_{sk}$ evaluated from Eq. (14) is 1.59 sec. For a 3/4-inch sphere $A = 3/R = 3.16$ cm. If the skin diffusivity is arbitrarily chosen to be 0.005 cm²/sec, the required skin thickness is a reasonable 0.025 cm. The group $t/A(D_e)_{sk}$ should be insensitive to temperature. Using a constant value, line 3 in Fig. 10 shows the calculated E.F. at other temperatures. The agreement is poor. This suggests that the skin thickness or diffusivity would have to vary greatly with temperature, which is unlikely.

2. *Kinetic Errors (Blocking Effect)*

The second key assumption in the calculation concerns the applicability of particle rate data determined independently for use in the pellet. If the assumption is not valid, the deviation in Figs. 10 and 11, between $(E.F.)_{exptl}$ and line 1, requires that the rate for a particle *in* the pellet be less than for that for an unpelletted particle. It may be postulated that the molding process partially blocks some of the micropore mouths and produces a skin effect on the outer surface of the particles. This is more likely for the soft, microporous alumina particles than it would be for solid, hard particles which are difficult to pellet. A blocking, or activity factor, γ may be defined to describe this situation:

$$\gamma = r_p^0/r_p \quad (15)$$

where r_p^0 is the rate for a blocked particle in the pellet. We may apply the temperature test to this effect by first calculating the value of γ necessary to give agreement with the experimental E.F. at 370°C. Here D_e from Table 5 is used so that the entire error in $(E.F.)_{calc}$ is supposed to be due to the blocking factor. The required value of γ is defined by Eq. (8) where the particle rate is given by Eq. (15). Hence,

$$(E.F.)_{exptl} = \frac{3}{(r_p)_s}\int_0^1 z^2 r_p^0 dz = \frac{3}{(r_p)_s}\int_0^1 z^2(\gamma r_p)dz \quad (16)$$

Assuming γ is constant for a given density, comparison of Eqs. (8) and (16) shows that

$$\gamma = \frac{(E.F.)_{exptl}}{(E.F.)_{calc}} \quad (17)$$

Applying Eq. (17), γ for Pellet 4 at 370°C is 0.62. Using this γ, the E.F. was calculated for other temperatures by numerical solution of Eqs. (5)–(7) and (8) with r_p^0 substituted for r_p. The result is designated as curve 4 in Fig. 10. This curve agrees better with the experimental result than curves 2 or 3. If the blocking effect is a valid concept, γ should increase with decreasing density. Table 7 shows that γ for the four density levels does increase, but only a small amount.

TABLE 7
BLOCKING FACTORS AT 370°C

Pellet density, $\bar{\rho}_B$ (g/cm³)	γ
0.68	0.73
0.79	0.69
0.91	0.63
1.11	0.62

Intraparticle Temperature Differences

The observed ΔT between the center of the pellet and the surface were small and hence, of uncertain accuracy. However, they do add additional information on the nature of the disagreement between $(E.F.)_{exptl}$ and $(E.F.)_{calc}$. Weisz and Prater (*21*) note that the Damkoehler expression for $T_c - T_s = \Delta T$ is valid for any rate equation and may be written

$$\Delta T = \frac{(-\Delta H)D_e(C_s - C_c)}{k_e} = \frac{(-\Delta H)D_eC_s(1 - \beta_c)}{k_e} \quad (18)$$

If the concentration of CO at the center is zero, the maximum ΔT results

$$(\Delta T)_{max} = \frac{(-\Delta H)D_eC_s}{k_e} \quad (19)$$

All the quantities in Eq. (19) are accurately known or measured except D_e. Using the diffusivities in Table 5, the $(\Delta T)_{max}$ obtained for Pellets 1 and 4 are those shown in the first row of Table 8. They are much higher than the experimental values given in the bottom row. Since the concentration of CO at the pellet center is available from the numerical solution of Eqs. (5)–(7), a more appropriate ΔT can be evaluated using Eq. (18). These results, in the third row, are still more than twice the observed temperature differences. This independent evidence of the reliability of $(E.F.)_{exptl}$ reinforces the argument that the errors are in the calculated effectiveness factors.

Conclusions

For the optimum design of pelletted catalysts it is necessary to be able to predict the rate of reaction per pellet from transport properties of porous media and rates of reaction in individual catalyst particles. The results of this experimental study indicate that this could not be accomplished reliably for large spherical pellets. The reason for the divergence between predicted and experimental effectiveness factors is not clear. Errors can exist in predicted results because of uncertainties in the diffusivities, but this does not appear to be a complete explanation. Viewed from the reaction rate standpoint, the experimental results suggest that the pelletting process reduces the activity of the catalyst. A blocking factor is introduced to describe this possibility quantitatively. Comparison of experimental and predicted effectiveness factors using this concept indicate that it may be a partial explanation of the anomalous results.

TABLE 8
Intraparticle Temperature Differences

Pellet No.		Temperature (°C)				
		370°	350°	325°	300°	275°
1	$(\Delta T)_{mac}$	43.9	43.2	42.6	41.6	40.6
	$1-\beta_c$	0.30	0.22	0.15	0.09	0.05
	$(\Delta T)_{calc}$	13.1	9.7	6.3	3.7	2.2
	$(\Delta T)_{exptl}$	6.5	4.6	2.8	1.6	0.9
4	$(\Delta T)_{mac}$	9.0	9.0	9.0	9.0	9.0
	$1-\beta_c$	0.80	0.66	0.50	0.33	0.17
	$(\Delta T)_{calc}$	7.3	5.9	4.5	3.0	1.6
	$(\Delta T)_{exptl}$	3.3	2.6	1.7	1.1	0.7

Acknowledgments

The financial assistance of the Petroleum Research Fund of the American Chemical Society for this research is gratefully acknowledged. Also the authors wish to thank Professor P. L. Silveston who participated in the discussion of some parts of this work.

References

1. Carberry, J. J., *A.I.Ch.E.* (*Am. Inst. Chem. Eng.*) **7**, 350 (1961).
2. Ibid. **7**, 350 (1961).
3. Cunningham, R. E., Carberry, J. J., and Smith, J. M., *A.I.Ch.E. J.* **11**, 636 (1965).
4. Keier, N. P., *et al. Dokl. Akad. Nauk. SSSR* **106**, 859 (1946).
5. Kirk, R. E., and Othmer, D. F., eds., "Encyclopedia of Chemical Technology" Vol. 1, p. 641. McGraw-Hill, New York, 1962.
6. Kubota, H., and Shindo, M., *Chem. Eng.* (*Tokyo*) **20**, 11 (1956).
7. Mingle, J. O., and Smith, J. M., *A.I.Ch.E. J.* **7**, 243 (1961).
8. Mischke, R. A., and Smith, J. M., *Ind. Eng. Chem. Fundamentals* **1**, 288 (1962).
9. Otani, S., Wakao, N., and Smith, J. M., *A.I.Ch.E. J.* **11**, 435, 446 (1965).
10. Parravano, G., and Boudart, M., *Advan. Catalysis* **7**, 50 (1955).
11. Rao, R. M., and Smith, J. M., ***A.I.Ch.E. J.*** **9**, 485 (1963).
12. Rao, R. M., and Smith, J. M., *A.I.Ch.E. J.* **10**, 293 (1964).
13. Satterfield, C. N., and Saraf, S. K., "Anisotropic Diffusivities in Pressed Catalyst Pellets." *Ind. Eng. Chem. Fundamentals,* to be published.
14. Thiele, E. W., *Ind. Eng. Chem.* **31**, 316 (1939).
15. Tinkler, J., and Pigford, R. L., *Chem. Eng. Sci.* **15**, 326 (1961).
16. Tinkler, J., and Metzner, A. B., *Ind. Eng. Chem.* **53**, 663 (1961).
17. Wagner, V. C., and Hauffe, K., *Z. Electrochem.* **44**, 172 (1938).
18. Wakao, N., Oshima, T., and Yagi, S., *Chem. Eng.* (*Tokyo*) **22**, 780 (1958).
19. Wakao, N., and Smith, J. M., *Chem. Eng. Sci.* **17**, 825 (1962).
20. Weisz, P. B., and Hicks, J. S., *Chem. Eng. Sci.* **17**, 265 (1962).
21. Weisz, P. B., and Prater, C. D., *Advan. Catalysis* **6**, 143 (1954).
22. Wheeler, A., *Catalysis* **2**, 105 (1955).
23. Winter, E. R. S., *Advan. Catalysis* **10**, 196 (1958).